Inorganic Chemistry

Article

pubs.acs.org/IC

A Eu^{III} Tetrakis(β-diketonate) Dimeric Complex: Photophysical Properties, Structural Elucidation by Sparkle/AM1 Calculations, and Doping into PMMA Films and Nanowires

Silvanose Biju,*[,†] Ricardo O. Freire,[‡] Yu Kyung Eom,[†] Rosario Scopelliti,[§] Jean-Claude G. Bünzli,*[,†,§] and Hwan Kyu Kim*[,†]

[†]Department of Advanced Materials Chemistry and WCU Center for Next Generation Photovoltaic Systems, Korea University, Jochiwon-eup, Sejong-si, 339-700 Republic of Korea

[‡]Pople Computational Chemistry Laboratory, Departamento de Química, Universidade Federal de Sergipe, 49.100-000 — São Cristóvão, SE Brazil

[§]Institut des Sciences et Ingénierie Chimiques, École Polytechnique Fédérale de Lausanne, BCH 1402, CH-1015 Lausanne, Switzerland

Supporting Information

ABSTRACT: Reaction of Ln^{III} with a tetrakis(diketone) ligand H_4L [1,1′-(4,4′-(2,2-bis((4-(4,4,4-trifluoro-3-oxobutanoyl) phenoxy)methyl)propane-1,3-diyl)bis(oxy)bis(4,1-phenylene))bis(4,4,4-trifluorobutane-1,3-dione)] gives new podates which, according to mass spectral data and Sparkle/AM1 calculations, can be described as dimers, $(NBu_4[LnL])_2$ (Ln = Eu, Tb, Gd:Eu), in both solid-state and dimethylformamide (DMF) solution. The photophysical properties of the Eu^{III} podate are compared with those of the mononuclear diketonate ($NBu_4[Eu(BTFA)_4]$, BTFA = benzoyltrifluoroacetonate), the crystal structure of which is also reported. The new Eu^{III} dimeric complex displays bright red luminescence upon irradiation at the ligand-centered band in the range of 250−400 nm, irrespective of the medium. The emission quantum yields and the luminescence lifetimes of $(NBu_4[EuL])_2$ (solid state: 51% ± 8% and 710 ± 2 μs; DMF: 31% ± 5% and 717 ± 1 μs) at room temperature are comparable to those obtained for $NBu_4[Eu(BTFA)_4]$ (solid state: 60 ± 9% and 730 ± 5 μs; DMF: 30 ± 5% and 636 ± 1 μs). Sparkle/AM1 calculations were utilized for predicting the ground-state geometries of the Eu^{III} dimer. Theoretical Judd−Ofelt and photoluminescence parameters, including quantum yields, predicted from this model are in good agreement with the experimental values, proving the efficiency of this theoretical approach implemented in the LUMPAC software (http://lumpac.pro.br). The kinetic scheme for modeling energy transfer processes show that the main donor state is the ligand triplet state and that energy transfer occurs on both the $^5D_1$ (44.2%) and $^5D_0$ (55.8%) levels. Furthermore, the newly obtained Eu^{III} complex was doped into a PMMA matrix to form highly luminescent films and one-dimensional nanowires having emission quantum yield as high as 67%−69% (doping concentration = 4% by weight); these materials display bright red luminescence even under sunlight, so that interesting photonic applications can be foreseen.

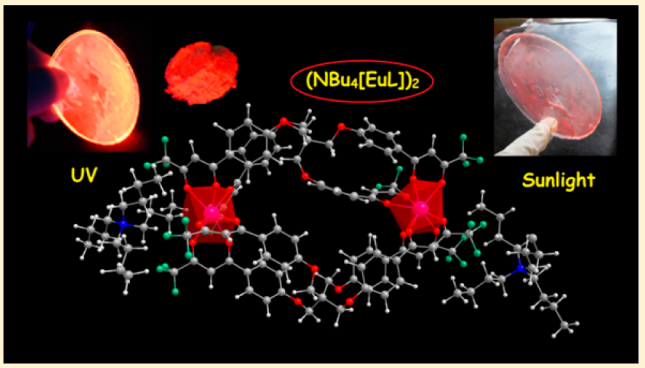

INTRODUCTION

Eu^{III} complexes involving fluorinated β-diketonates are known to give bright red emission under near-ultraviolet or visible-light irradiation, because of efficient energy transfer from the β-diketonate ligand to the central Eu^{III} ions (antenna effect).[1,2] Their unique optical properties, such as large antenna-generated (Richardson) shifts,[3] monochromaticity, high luminescence efficiency, and long excited-state lifetimes make them of interest for a wide range of photonic applications including light-emitting diodes,[4] lasers,[4b,5] luminescent solar concentrators, wavelength-converting layers for photovoltaic cells,[6,7] and luminescent probes for bioanalyses and medical imaging.[8] Fluorinated β-diketonates with organic chromophores such as thenyl (TTA), phenyl (BTFA), and naphthyl (NTA) are among the best ligands for sensitizing Eu^{III} luminescence and have several advantages over nonfluorinated β-diketonates.[9] Reported Eu^{III} complexes with these ligands include mononuclear hexacoordinate neutral binary (tris), octacoordinated neutral ternary (adducts of tris), and octacoordinated anionic (tetrakis) complexes. Among them, the luminescence efficiency follows the order tris < tris-adduct < tetrakis. As an extension of the initial ligands, bis(β-diketonates) have been proposed, either for now well-

Received: April 25, 2014
Published: July 28, 2014

   dx.doi.org/10.1021/ic500966z | Inorg. Chem. 2014, 53, 8407−8417

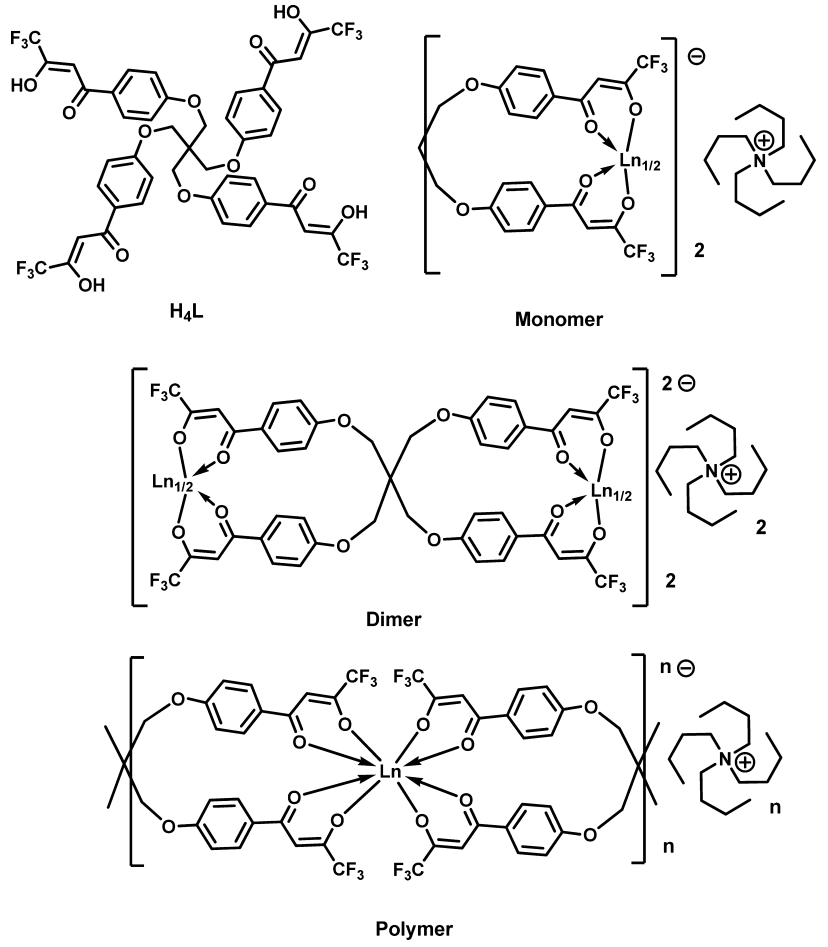

Figure 1. Chemical formula of the ligand H_4L and possible chemical structures of its Ln^{III} complexes.

established bioanalyses[10] or for isolating dinuclear Eu^{III} complexes. The latter are attracting much attention, because of their high thermal stability,[11] excellent photoluminescent and electroluminescent properties,[11,12] formation of helical structures,[12a,13] and visible-light sensitization.[14]

Since lanthanide β-diketonates have limited thermodynamic stability in solution, we have recently designed a fluorinated tetrakis(β-diketone) podand H_4L in order to benefit from an enhanced chelate effect. The new ligand combines four benzoyltrifluoroacetone (BTFA) moieties anchored to a single carbon atom (Figure 1); it wraps around Ln^{III} cations, saturating their coordination sphere, efficiently shielding them from solvent interaction, and showing excellent sensitization efficiency of Sm^{III} and Yb^{III} luminescence.[15] In this paper, we now extend this work by testing the ability of H_4L to sensitize Eu^{III} and Tb^{III} luminescence and by trying to unravel the exact structure of the Eu^{III} podate both experimentally and by means of theoretical Sparkle/AM1 calculations. Structural and photophysical data are also compared with those of a reference tetrakis β-diketonate, $NBu_4[Eu(BTFA)_4]$.

The Eu^{III} podate appears to be highly luminescent, so that a second objective is to insert it into a polymeric matrix in order to produce easily processable and highly luminescent materials. Indeed, major shortcomings preventing Eu^{III} β-diketonates from practical usage are their inability to withstand high temperature, high pressure, or moisture, as well as their low mechanical resistance.[4b,16] Most of these problems can be cured by making organic−inorganic hybrid[4b] photoemissive materials. These occupy a place of choice in the search for new red-emissive materials, because they do not need high-temperature synthesis, as inorganic phosphors necessitate, and, moreover, they can be processed using inexpensive and viable techniques.[17] Such materials are made of a molecular Eu^{III} complex either covalently linked to the organic matrix or doped into the matrix. In the latter case, a commonly used polymer is poly(methyl methacrylate) (PMMA), since it is inexpensive and optically transparent, so that it can be regarded as a glass analogue.[18] For instance, McCoy et al. recently designed a pH sensor by the irreversible incorporation of a Eu^{III}- quinoline-cyclen conjugate complex into water-permeable hydrogels using poly[methyl methacrylate-*co*-2-hydroxyethyl methacrylate]-based hydrogels.[19] In addition, one-dimensional (1D) nanostructures also have drawn much attention recently, because of their importance for both fundamental studies and technological applications.[20] A large number of synthesis and fabrication methods have been demonstrated for generating 1D nanostructures in the form of fibers, wires, rods, belts, tubes, spirals, and rings from various materials.[20] Among these methods, electrospinning is catching interest as a simple electrostatic method for generating 1D nanostructures from organic−inorganic materials.[21] Thus, in the present work, we dope the newly developed Eu^{III} podate into a PMMA matrix to obtain highly transparent films that are subsequently electrospun to form 1D nanowires with excellent optical properties.

dx.doi.org/10.1021/ic500966z | Inorg. Chem. 2014, 53, 8407−8417

EXPERIMENTAL SECTION

Materials. Lanthanide(III) nitrate hexahydrates (99.9%) (Ln = Eu, Gd, Tb) were obtained from Sigma–Aldrich. Benzoyltrifluoroacetone (99.9%, Sigma–Aldrich), tetra-*n*-butylammonium bromide 99.9% (Acros Organics), and PMMA (99.9%, Sigma–Aldrich) were used without further purification. Solvents were dried using standard methods. All the other chemicals used were of analytical reagent grade. The ligand H_4L was prepared as described previously.[15]

Synthesis of the Ln^{III} Complexes. The reference Eu^{III} complex $NBu_4[Eu(BTFA)_4]$ and the Ln^{III} podates $NBu_4[LnL]$ were synthesized according to reported procedures.[5,15] Colorless needles of $NBu_4[Eu(BTFA)_4]$ suitable for X-ray diffraction were obtained by slow evaporation of a concentrated solution of the complex in absolute alcohol. The poor solubility of the $NBu_4[LnL]$ podates in common organic solvents prevented the formation of single crystals. These complexes were soluble only in dimethylformamide (DMF) and dimethyl sulfoxide (DMSO) and efforts to grow single crystals from solvent combinations involving DMF and DMSO were not successful.

$NBu_4[Eu(BTFA)_4]$ (colorless solid). Yield: 95%. Elemental analysis (%) calcd. for $C_{56}H_{60}EuF_{12}NO_8$ (1255.02): C, 53.59; H, 4.82; N, 1.12. Found: C, 53.83; H, 4. 94; N, 1.20. FTIR (KBr) ν_{max} (cm^{-1}): 3069 (ν, $C_{sp2}H$); 2969, 2938, 2881 (ν, $C_{sp3}H$); 1616, 1577 (ν_s, C=O); 1530, 1491, 1319 (ν, C=C);1188, 1136, (δ, C–H); 1110 (ν_s, C–F); 1023 (ν_s, C–N); 855, 763 (δ, C–H), 700 (δ, CF_3).

$NBu_4[EuL]$ (yellow solid). Yield: 95%. Elemental analysis (%) calcd. for $C_{61}H_{64}EuF_{12}NO_{12}$ (2766. 21): C, 52.97; H, 4.66; N, 1.01. Found: C, 53.23; H, 4. 94; N, 1.11. FTIR (KBr) ν_{max} (cm^{-1}): 3070 (ν, $C_{sp2}H$); 2965, 2938, 2877 (ν, $C_{sp3}H$); 1678, 1626 (ν_s, C=O); 1598, 1500, 1470, 1308 (ν, C=C); 1288, 1244 (ν_s, C–O); 1173, 1124 (δ, C–H); 1118 (ν_s, C–F); 1015 (ν_s, C–N); 840, 781 (δ, C–H), 704 (δ, CF_3).

$NBu_4[Gd_{0.96}Eu_{0.04}L]$ (yellow solid). Yield: 93%. Elemental analysis (%) calcd. for $C_{61}H_{64}Eu_{0.04}F_{12}Gd_{0.96}NO_{12}$: C, 52.79; H, 4.66; N, 1.01 found: C, 53.01; H, 4.81; N, 1.05. FTIR (KBr) ν_{max} (cm^{-1}): 3070 (ν, $C_{sp2}H$); 2967, 2940, 2879 (ν, $C_{sp3}H$); 1671, 1631 (ν_s, C=O); 1601, 1500, 1468, 1309 (ν, C=C); 1281, 1236 (ν_s, C–O); 1173, 1125 (δ, C–H); 1113 (ν_s, C–F); 1021 (ν_s, C–N); 845, 783 (δ, C–H), 703 (δ, CF_3).

$NBu_4[TbL]$ (yellow solid). Yield: 95%. Elemental analysis (%) calcd. for $C_{61}H_{64}TbF_{12}NO_{12}$ (2780.13): C, 52.71; H, 4.64; N, 1.01 found: C, 52.93; H, 4. 88; N, 1.15. FTIR (KBr) ν_{max} (cm^{-1}): 3070 (ν, $C_{sp2}H$); 2966, 2939, 2877 (ν, $C_{sp3}H$); 1678, 1626 (ν_s, C=O); 1598, 1500, 1470, 1308 (ν, C=C); 1287, 1244 (ν_s, C–O); 1173, 1124 (δ, C–H); 1116 (ν_s, C–F); 1015 (ν_s, C–N); 840, 781 (δ, C–H), 703 (δ, CF_3).

Synthesis of the PMMA Films and Nanowires. The PMMA films were obtained by drop casting and the wires were prepared with the eS-Robot electrospinning system from NanoNc Co. Ltd., Korea. DMF solutions of PMMA doped with 4 wt % of Eu^{III} complexes were introduced in a syringe with a needle of gauge 23 G and electrospun by applying a voltage of 8 kV between the solution and the counter electrode was kept at a distance of 10 cm.

Crystal Structure Determination. Single-crystal X-ray diffraction (XRD) data for $NBu_4[Eu(BTFA)_4]$ were collected at room temperature using Cu Kα radiation on an Agilent Technologies SuperNova dual system in combination with an Atlas CCD detector. The data reduction was carried out by Crysalis PRO.[22a]

The solution and refinement were performed by SHELX.[22b] The crystal structure was refined using full-matrix least-squares based on F^2 with all non-hydrogen atoms anisotropically defined. Hydrogen atoms were placed in calculated positions by means of the "riding" model. CCDC-977079 contains supplementary crystallographic data for the complex. These data can be obtained free of charge via the Internet at www.ccdc.cam.ac.uk/conts/retrieving.html [or from the Cambridge Crystallographic Data Centre, 12 Union Road, Cambridge CB2 2EZ, U.K.; Fax: +44-1223/336033; E-mail: deposit@ccdc.cam.ac.uk)].

Methods. Elemental analyses were performed with a Perkin–Elmer Series 2 Elemental Analyzer 2400. IR spectral data were recorded on KBr (neat) disks with a Perkin–Elmer Spectrum One FT-IR spectrometer. Matrix-assisted laser desorption ionization time-of-flight (MALDI-TOF) mass spectra were recorded on KRATOS analytical spectrometer (Shimadzu, Inc.) and the thermogravimetric analyses were performed on a Model TGA-50H instrument (Shimadzu, Japan). Absorbances of the ligands, complexes in PMMA and in DMF solutions were measured on a Model UV-2450 spectrophotometer (Shimadzu). Photoluminescence spectra were recorded on a Fluorolog FL 3-22 spectrometer from Horiba-Jobin Yvon-Spex equipped for both visible and NIR measurements and were corrected for the instrumental function. Powdered samples were put into 2 mm i.d. quartz capillaries. The PMMA films with a size of ~10 mm × 5 mm were used as such and solution studies were conducted using 10-mL quartz cuvettes. Overall quantum yield (QY) data were determined at room temperature (rt) on the same instrument using a home-modified integrating sphere;[23] PMMA films with a thickness of 0.5–0.9 mm were used for these determinations. The values reported are averages of six different measurements and the estimated error is ±15%. Lifetime measurements were carried out at rt, using a Spex 1040 D phosphorimeter.

Experimental Judd–Ofelt Parameters. The intensity parameters Ω_λ for $NBu_4[Eu(BTFA)_4]$ and $(NBu_4[EuL])_2$ were determined from their emission spectra, using the relationship:

$$\Omega_\lambda = \frac{4e^2\omega^3 A_{0J}}{3\hbar\chi\langle {}^7F \| U^\lambda \| {}^5D_0\rangle^2} \quad (1)$$

where A_{0J} is the coefficient of spontaneous emission for the $^5D_0 \rightarrow {}^7F_J$ transition, χ is the Lorentz local-field correction term (given by $\chi = (n(n^2+2)^2)/9$, where n is the refractive index of the medium (in this case, $n = 1.5$)), and U is the square reduced matrix element whose values are 0.0032, 0.0023, and 0.0002 for $\lambda = 2$, 4, and 6, respectively.[24] The transition $^5D_0 \rightarrow {}^7F_6$ is not observed experimentally; thus, the experimental Ω_6 parameter cannot be estimated.

RESULTS AND DISCUSSION

Characterization. Microanalytical data for the Ln^{III} complexes demonstrate that the Ln:ligand mole ratio is 1:1 in $NBu_4[LnL]$ and 1:4 in $NBu_4[Eu(BTFA)_4]$, whereas the Ln:$[NBu_4]^+$ mole ratio remains 1:1 in all of the complexes studied. The IR carbonyl stretching frequency of free ligands ($\nu_{s(C=O)}$ = 1607 cm^{-1} in HBTFA and 1600 cm^{-1} in H_4L)[15] shifts to 1616–1626 cm^{-1} in the complexes along with the appearance of new peaks in the range 1671–1678 cm^{-1}, thus indicating coordination of the carbonyl groups to the Ln^{III} cation in each case. The FT-IR spectra of all the isolated Ln^{III} complexes also feature signals in the range of 2800–2900 cm^{-1}, because of the $-CH_2-$ groups and ~1015–1017 cm^{-1}, $\nu_{s(C-N)}$, thus confirming the presence of $[NBu_4]^+$ as counterion. This observation along with the absence of any broad absorption band at ~3200–3500 cm^{-1} for the Ln^{III} complexes confirm that they are devoid of water molecules and, therefore, that all the coordination sites are occupied by β-diketonate moieties. Thermogravimetric analysis under nitrogen atmosphere (see Figure S1 in the Supporting Information) shows that the starting decomposition temperature of $NBu_4[Eu(BTFA)_4]$ (220 °C) is slightly higher than the one for $NBu_4[LnL]$ (200 °C). Upon further heating, the thermal behaviors of $NBu_4[Eu(BTFA)_4]$ and $NBu_4[LnL]$ are different. For $NBu_4[Eu(BTFA)_4]$, weight loss mainly occurs in two sharp steps (310 and 490 °C) and decomposition is complete at 700 °C. On the other hand, $NBu_4[LnL]$ podates decompose in a more-complex way with broader steps in the range 210–310, 330–600, and 630–800 °C. The residual weights are between ~14%–17% of the initial mass and are found to be slightly larger than calculated for the formation of the corresponding Ln_2O_3 (~13%–15%). This may be attributed to partial formation of

dx.doi.org/10.1021/ic500966z | Inorg. Chem. 2014, 53, 8407–8417

lanthanide fluorides or oxyfluorides, which is a common phenomenon among Ln^{III} fluorinated β-diketonates.

Finally, mass spectral analysis of solid-state $NBu_4[LnL]$ samples (Ln = Eu^{III}, Tb^{III}) shows peaks at m/z = 2327.13 (40%) $(Na_2[Eu_2L_2])^+$, 1164.04 (65%) $(Na[EuL])^+$, 2341.11 (35%) $(Na_2[Tb_2L_2]+H)^+$, 1171.06 (70%) $(Na[TbL]+H)^+$ (see Table S1 in the Supporting Information). Such mass spectral data suggest that the podates may exist as $(NBu_4[LnL])_2$ dimers in solid state, as some other theoretical and experimental data will confirm later. Therefore, from now on, a dimeric structure is adopted to describe the podates.

Crystal Structure of $NBu_4[Eu(BTFA)_4]$. This complex crystallizes in the monoclinic space group $P2_1/c$. The asymmetric unit consists of two independent $NBu_4[Eu(BTFA)_4]$ molecules, having only slightly different coordination environments for Eu^{III}. One of them (corresponding to Eu1), is displayed in Figure 2, along with its partial numbering scheme.

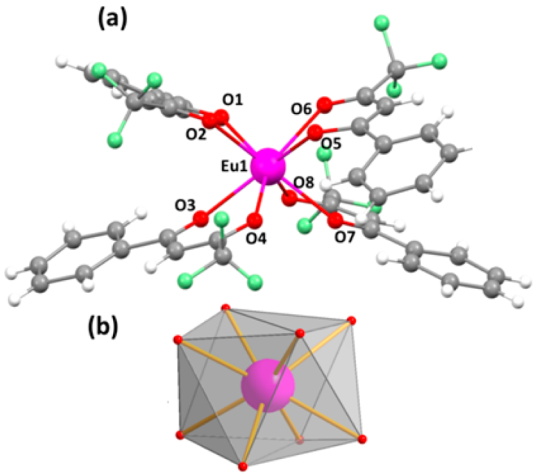

Figure 2. (a) Perspective view of $NBu_4[Eu(1)(BTFA)_4]$, (b) Coordination polyhedron of the central $Eu^{III}(1)$ ion: the countercation $[NBu_4]^+$ is not shown for the sake of clarity.

Relevant experimental parameters are listed in Table S2 in the Supporting Information, and selected bond lengths [Å] and angles [°] are given in Table 1. As can be seen from Figure 2, the Eu^{III} ion is surrounded by eight oxygen atoms, provided by four bidentate β-diketonate moieties. The mean Eu−O distance amounts to 2.38(4) Å, very close to the median value observed for analogous compounds with *O,O*-chelating β-diketonates: 2.37 Å (96 structures).[9a] In order to gain better insight into the coordination geometry around the Eu(1) ion and estimate the degree of distortion from ideal 8-coordination polyhedra, the "shape measure" criterion S (eq 2)[25] was employed:

$$S = \min\left(\sqrt{\frac{1}{m}\sum_{i=1}^{m}(\delta_i - \theta_i)^2}\right) \quad (2)$$

A thorough investigation of the data shows that coordination around Eu^{III} deviates substantially from the ideal polyhedra for bicapped trigonal prism (C_{2v}, S = 21.77) and trigonal dodecahedron (D_{2d}, S = 15.28) while a smaller deviation is obtained for square antiprism (D_{4d}, S = 5.03). Thus, the coordination polyhedron around the Eu^{III} ions can be best described as a distorted square antiprism (SAP, Figure 2b). The square faces formed by the oxygen atoms of the SAP are separated by 2.58 Å and are tilted by 1.6°, while the average dihedral angle amounts to 45.1°.

Structures of the Eu^{III} Podate Calculated with the Sparkle/AM1 Model. In the absence of single crystals for Ln^{III} podates, the semiempirical Sparkle/AM1 model was used to calculate the ground-state geometries of the Eu^{III} complex. The octadentate L^{4-} anion and the Eu^{III} cation can form three different types of complexes (Figure 1) having the same ligand:metal ratio, 1:1, namely, a monomer $NBu_4[LnL]$, a dimer $(NBu_4[LnL])_2$, and a coordination polymer $(NBu_4[LnL])_n$. The ground-state geometry obtained for the monomer showed large deviation from planarity for the aromatic rings in L^{4-} (see Figure S2 in the Supporting Information), so that one can probably rule out the formation of this highly strained species. This does not occur in the two other structures, the calculated ground-state geometries of which are shown in Figure 3 (dimer) and Figure S3 (polymer)

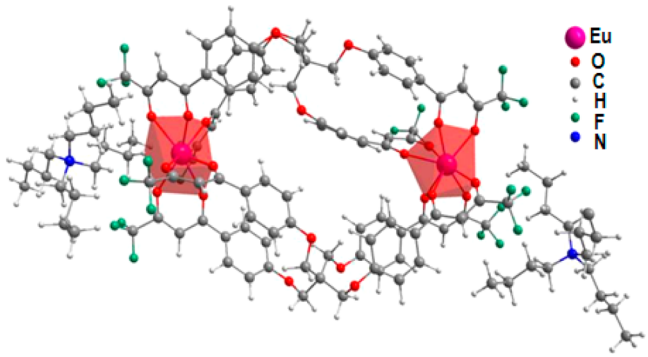

Figure 3. Ground-state geometry of $(NBu_4[EuL])_2$ calculated using the Sparkle/AM1 model.

in the Supporting Information). The corresponding calculated spherical atomic coordinates, charge factors (g), and polarizability (α) of the oxygen atoms bound to the metal ion are summarized in Table 2 (dimer) and Table S3 (polymer) in the Supporting Information). The average Eu−O bond lengths, 2.396 Å for the dimer and 2.394 Å for the polymer are very similar and are in good agreement with the value (2.385 Å) obtained for $NBu_4[Eu(BTFA)_4]$ by X-ray analysis. Since MS data reported above do not show the presence of oligomers larger than dimers; therefore, we keep to the latter structure in the following descriptions.

Table 1. Selected Bond Lengths and Bond Angles for $NBu_4[Eu(BTFA)_4]$[a]

Bond Lengths				Bond Angles	
bond	value (Å)	bond	value (Å)	bond angle	value (°)
Eu(1)−O(1)	2.368(8)	Eu(1)−O(5)	2.369(7)	O(1)−Eu(1)−O(2)	69.4(3)
Eu(1)−O(2)	2.433(8)	Eu(1)−O(6)	2.393(7)	O(3)−Eu(1)−O(4)	70.1(3)
Eu(1)−O(3)	2.366(6)	Eu(1)−O(7)	2.372(8)	O(5)−Eu(1)−O(6)	70.9(3)
Eu(1)−O(4)	2.397(8)	Eu(1)−O(8)	2.399(8)	O(7)−Eu(1)−O(8)	70.6(3)

[a]These values refer to the Eu(1) molecule only.

dx.doi.org/10.1021/ic500966z | Inorg. Chem. 2014, 53, 8407−8417

Table 2. Spherical Atomic Coordinates of the Oxygen Atoms Bound to Eu^{III} in $(NBu_4[EuL])_2$, Charge Factors (g), and Polarizability (α) of the Coordinated Atom

atom	R (Å)	θ (°)	ϕ (°)	g^a	α^a
O1 (β-diketone 1)	2.39450	54.681	24.175	0.1211	2.4996×10^{-24}
O2 (β-diketone 1)	2.38826	73.099	318.618	0.0111	6.4980×10^{-24}
O1 (β-diketone 2)	2.40273	122.417	177.626	0.1211	2.4996×10^{-24}
O2 (β-diketone 2)	2.39024	163.979	283.260	0.0111	6.4980×10^{-24}
O1 (β-diketone 3)	2.39779	88.455	108.629	0.1211	2.4996×10^{-24}
O2 (β-diketone 3)	2.40172	126.069	54.081	0.0111	6.4980×10^{-24}
O1 (β-diketone 4)	2.39933	41.400	222.271	0.1211	2.4996×10^{-24}
O2 (β-diketone 4)	2.39322	96.843	253.000	0.0111	6.4980×10^{-24}

[a]Obtained using a nonlinear minimization technique.

Electronic Absorption Spectroscopy. One of the most important criteria for an organic molecule to act as an efficient sensitizer for Ln^{III} luminescence is that it must have a high molar absorption coefficient. Hence, absorption spectra have been recorded for the newly synthesized complexes at room temperature in DMF solution, as well as in PMMA films; they are displayed in Figure 4 and relevant data are gathered in

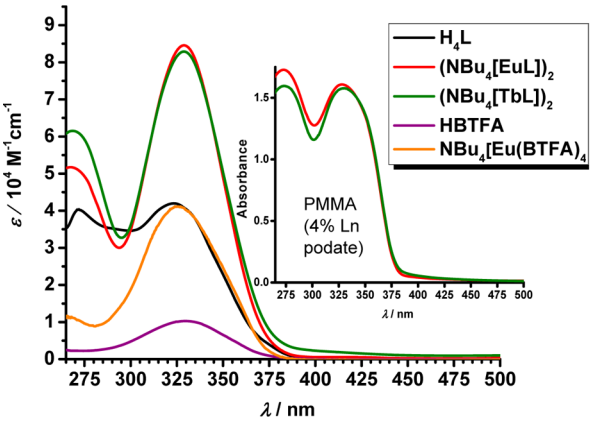

Figure 4. UV–vis absorption spectra of HBTFA, H_4L, and their complexes in DMF at 298 K; ($c \approx 2 \times 10^{-6}$ M except for $(NBu_4[LnL])_2$, 1×10^{-6} M). Insert: spectra of PMMA films 4 wt % doped with $(NBu_4[LnL])_2$ (thickness ≈ 0.6–0.7 mm).

Table 3. From Figure 4, it is evident that the absorption spectrum of H_4L shows two maxima at 323 and 272 nm ($\varepsilon \approx$ 40–42 000 M^{-1} cm^{-1}), whereas the signal obtained for HBTFA shows a single maximum at 329 nm (ε = 10 270 M^{-1} cm^{-1}). The peaks at ~323 nm in H_4L and ~329 nm in HBTFA can be attributed to the singlet–singlet ($^1\pi-\pi^*$) enolic transitions of the β-diketone moieties,[13a] while the features present in H_4L at lower wavelengths are due to singlet–singlet ($^1\pi-\pi^*$) transitions in the phenyl rings.[13a] Substitution of alkoxy group at the para-position of the phenyl ring of the HBTFA moieties enlarges the degree of conjugation and is responsible for the slight red shift in the absorption maximum in H_4L. The absorption spectra of both lanthanide podates $(NBu_4[LnL])_2$ (Ln = Eu, Tb) are similar to that of H_4L, except for a small blue shift of the band at 272 nm to 268–269 nm and a red shift of the 323 nm absorption maximum to 328–329 nm. This is in accordance with the fact that conjugation in the β-diketonate moieties becomes larger upon coordination with Ln^{III} ions. On the other hand, the absorption spectrum of $NBu_4[Eu(BTFA)_4]$ shows a small blue shift (4 nm) in absorption maxima, when compared to free HBTFA. Furthermore, the molar absorption coefficients of the lowest-energy transition calculated for H_4L and $NBu_4[Eu(BTFA)_4]$ are similar (~40–42 000 M^{-1} cm^{-1}) and four times higher than that for HBTFA (10 270 M^{-1} cm^{-1}) pointing to the presence of four BTFA moieties in these entities. Finally, the molar absorption coefficients calculated if a dimeric structure is supposed for $(NBu_4[LnL])_2$ (Ln = Eu, Tb) are as high as 82 830–84 560 M^{-1} cm^{-1}. The absorption spectra of thin films of PMMA doped with 4 wt % of $(NBu_4[LnL])_2$ (Ln = Eu, Tb) display two well-resolved signals at ~328 and 274 nm (Figure 4, inset). The overall shapes of the absorption spectra in DMF and PMMA are similar; hence, one can assume that the absorbing species remain the same in both media.

Table 3. UV-vis Absorption Spectral Data of the Ligands and Their Ln^{III} Complexes in DMF ($c \approx 2 \times 10^{-6}$ M except for $(NBu_4[LnL])_2$, 1×10^{-6} M) and 4 wt % Doped PMMA Films at 298 K

compound	λ_{max} (nm)[a]
H_4L	323 (41980), 272 (40360)
$(NBu_4[EuL])_2$	329 (84560), 268 (51710)
$(NBu_4[TbL])_2$	328 (82830), 269 (61540)
HBTFA	329 (10270)
$NBu_4[Eu(BTFA)_4]$	325 (41110)
$(NBu_4[EuL])_2$/PMMA 4 wt %	328, 274
$(NBu_4[TbL])_2$/PMMA 4 wt %	328, 274

[a]Data given in parentheses represent ε values (shown in units of M^{-1} cm^{-1}).

Luminescence Properties of the Complexes. Excitation spectra of the Eu^{III} complexes recorded at room temperature in solid state and in DMF solution by monitoring the Eu($^5D_0 \rightarrow {}^7F_2$) transition at 613 nm are depicted in Figure 5. Spectra recorded in DMF solution have similar shape with three maxima at 275–280, 314–318, and 350–355 nm. No Eu^{III}-centered excitation bands are seen, pointing to an efficient antenna effect. The solid-state spectra recorded under optically saturated conditions are somewhat broader, particularly for $NBu_4[Eu(BTFA)_4]$; they display the same two high-energy maxima as solutions (270–280 and 300–310 nm) while the third maximum is clearly red-shifted to 360–370 nm. The observed excitation bands may be assigned to excited states of the ligands or, possibly, to ligand-to-metal charge-transfer transitions. Apart from these broad features, some low-intensity f–f transitions, $^5D_2 \leftarrow {}^7F_{0,1}$ (464 nm) and $^5D_1 \leftarrow {}^7F_{0,1}$ (535 nm), can also be identified.

The steady-state, room-temperature emission spectra of $(NBu_4[EuL])_2$ and $NBu_4[Eu(BTFA)_4]$ in solid state and in DMF solution, obtained under excitation at the wavelength

dx.doi.org/10.1021/ic500966z | Inorg. Chem. 2014, 53, 8407–8417

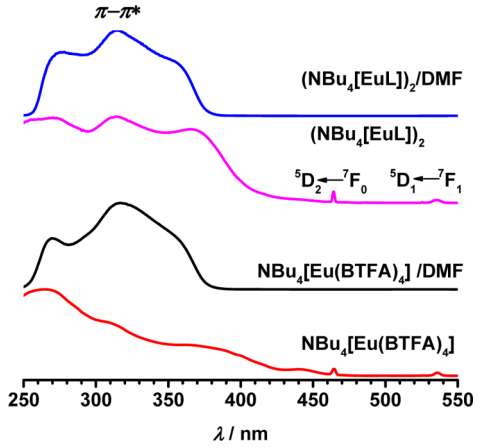

Figure 5. Excitation spectra of the Eu^{III} complexes at 298 K in solid state and in DMF ($c \approx (1–2) \times 10^{-6}$ M); emission is monitored at 613 nm; vertical scales are arbitrary units.

maximizing emission intensity (365 and 315 nm, respectively), are gathered in Figure 6a while relevant quantitative data are listed in Table 4. Emission spectra for both complexes are dominated by the typical Eu^{III}-centered lines, assigned to transitions between the $^5D_0$ excited state and the ground multiplet ($^7F_{0–4}$).[26] The emission spectra of the complexes show only one peak for the $^5D_0 \rightarrow {}^7F_0$ (0–0) transition and up to three Stark components for the magnetic dipole $^5D_0 \rightarrow {}^7F_1$ transition (Figure 6b), suggesting the presence of a single major chemical environment around the Eu^{III} ion.[3] A more-detailed analysis shows that there are substantial differences between spectra in solution and in the solid state. The case of $NBu_4[Eu(BTFA)_4]$ is interesting, in that the above crystal structure analysis points to a distorted D_{4d} symmetry. In this symmetry group (which does not contain an inversion center), the hypersensitive $^5D_0 \rightarrow {}^7F_2$ transition is forbidden,[27] as well as $^5D_0 \rightarrow {}^7F_0$. Distortions would lead, in a first step, to S_8, C_{4v}, or D_4 symmetries in which $^5D_0 \rightarrow {}^7F_2$ is allowed but only the latter symmetry forbids $^5D_0 \rightarrow {}^7F_0$, which is hardly experimentally observed. Overall, the emission spectrum is therefore compatible with an idealized D_4 symmetry, in particular the splitting of $^5D_0 \rightarrow {}^7F_2$ into two components. When the complex is dissolved into DMF, the intensity of the 0–0 transition increases by a factor 10 (Table 4) and the $^5D_0 \rightarrow {}^7F_1$ transition is clearly split into three components (Figure 6b), suggesting a lower symmetry. DMF is known to be a strong complexing agent for lanthanides and this spectrum may well reflect some dissociation of the complex with one β-diketonate unit replaced with DMF molecules. As a matter of fact, the energy of the 0–0 transition, $\tilde{\nu}(0–0) = 17\ 256\ cm^{-1}$, exactly matches the one reported for $[Eu(NO_3)(DMF)_x]^{2+}$ in DMF.[28] The situation for $(NBu_4[EuL])_2$ is somewhat different in that the spectrum of the solid-state sample displays a more intense 0–0 transition compared to the tetrakis complex (Table 4), as well as three components for the magnetic dipole transition, pointing to a low symmetry around the metal ion. However, when dissolved in DMF, the spectrum becomes very similar to that of the tetrakis complex, with identical $\tilde{\nu}(0–0)$ and with a splitting pattern of the $^5D_0 \rightarrow {}^7F_1$ transition matching that of the reference complex. Therefore, we can conclude that, in solution, the metal ion environment is very similar for the two Eu^{III} compounds.

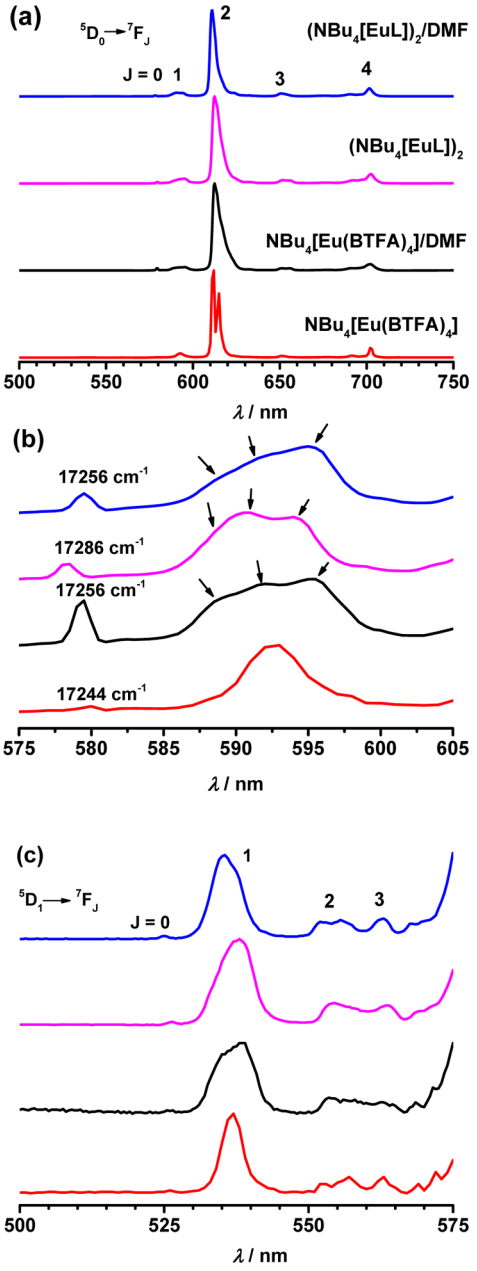

Figure 6. (a) Corrected emission spectra of the Eu^{III} complexes at 298 K in solid state (λ_{ex} = 365 nm) and in DMF ($c \approx 2 \times 10^{-6}$ M $NBu_4[Eu(BTFA)_4]$, and 1×10^{-6} M for $(NBu_4[EuL])_2$: λ_{ex} = 315 nm), (b) enlarged view of $^5D_0 \rightarrow {}^7F_{0–1}$ transitions (c) enlarged view of $^5D_1 \rightarrow {}^7F_{0–4}$ transitions; vertical scales are arbitrary units.

All the spectra are dominated by the hypersensitive $^5D_0 \rightarrow {}^7F_2$ transition (full width at half height, <10 nm). The intensity ratio of this forced electric dipole transition to the magnetic dipole transition $R = I(^5D_0 \rightarrow {}^7F_2)/I(D_0 \rightarrow {}^7F_1)$, in which I are integrated intensities of the transitions, is related to the presence or absence of an inversion center in the coordination sphere.[29] For $(NBu_4[EuL])_2$ and $NBu_4[Eu(BTFA)_4]$, R = 16.5 and 11.3 in solid state and 17.6 and 22.8 in DMF (Table 4). Such a high ratio is usually observed when the Eu^{III} ion occupies a site without inversion symmetry.[3,26]

A careful observation of the emission spectra of both Eu^{III} complexes shows some very low intensity peaks at higher energy due to emission from the $^5D_1$ state (Figure 6c). It is

dx.doi.org/10.1021/ic500966z | Inorg. Chem. 2014, 53, 8407–8417

Table 4. Relative Integrated and Corrected $^5D_0 \rightarrow {}^7F_J$ (J = 0−4) Transition Intensities for the Two Eu^{III} Complexes at 298 K in Solid State (λ_{ex} = 365 nm) and in DMF (λ_{ex} = 315 nm)[a]

	$NBu_4[Eu(BTFA)_4]$		$(NBu_4[EuL])_2$	
parameter	solid-state	DMF (2×10^{-6} M)	solid-state	DMF (1×10^{-6} M)
$\int_{0-0}$	0.01	0.1	0.04	0.03
$\int_{0-1}$	1	1	1	1
$\int_{0-2}$	11.3	22.8	16.5	17.6
$\int_{0-3}$	0.41	0.51	0.69	0.62
$\int_{0-4}$	2.34	2.56	2.23	2.56
$\int_{Total}$	15.03	26.97	20.46	21.81

[a]Estimated error = ±5%.

known that the energy difference $\Delta E(^5D_1—^5D_0)$ = 1700 cm^{-1} is approximately equal to the stretching frequency of the C═O group of bonded DMF molecule (~1650 cm^{-1}) so that DMF coordination favors internal $^5D_1 \rightarrow {}^5D_0$ conversion.[28] As a matter of fact, weak $^5D_1 \rightarrow {}^7F_J$ signals have been detected for nitrato complexes $[Eu(NO_3)_x(DMF)_y]^{(3-x)+}$ in DMF, but not for the solvate $[Eu(DMF)_y]^{3+}$.[28] Therefore, our observation of $^5D_1$ emission in the presently reported complexes tends to support the presence of some inner-sphere interaction of solvent molecules in DMF solutions.

It is generally accepted that Judd−Ofelt theory can be used to provide insight into the nature of the chemical bonding in Ln^{III} complexes.[30] Optical spectra are simulated with the help of empirical intensity (or Judd−Ofelt) parameters Ω_λ (λ = 2, 4, and 6). In particular, Ω_2 is especially sensitive to the symmetry around the metal ion and to the polarizability of the Ln^{III}−ligand bonds. In the case of Eu^{III}, Ω_2 and Ω_4 can be directly estimated from the oscillator strengths of the $^5D_0 \rightarrow {}^7F_J$ (J = 2, 4) transitions in the emission spectrum. The obtained values are listed in Table 5. The large values of Ω_2 might be interpreted as a consequence of the hypersensitive behavior of the $^5D_0 \rightarrow {}^7F_2$ transition[33] and suggest that the chemical environment is highly polarizable, as is the case for β-diketonates. The Ω_4 parameter is less sensitive to the coordination environment than Ω_2; however, its values reflect a rigid chemical environment surrounding the Eu^{III} cation.[31]

The rt lifetime values (τ_{obs}) of the $^5D_0$ level were determined by fitting the luminescence decay profiles with monoexponential functions, irrespective of the media. This is consistent with a single major emitting species in these materials. Lifetime values gathered in Table 5 show a 13% reduction in going from solid state to the solution for the tetrakis complex, from 730 ± 5 μs to 636 ± 1 μs. On the other hand, τ_{obs} values remain almost the same for $(NBu_4[EuL])_2$ in both media. This observation can be rationalized by the rigid structure of the dimeric podate, which restricts the thermal movement of the ligands and reduces the energy loss by radiationless decay. Furthermore, both complexes have ~1.9 times longer lifetimes in the solid state than $[Eu(BTFA)_3(H_2O)_2]$ (380 μs),[32] pointing to the absence of high-energy vibrators in the inner coordination sphere. However, lifetimes remain in the observed range for anhydrous β-diketonates, even in solution, pointing to a reduced influence of DMF (lifetimes for the DMF solvate and nitrato complexes are in the range of 1.36−1.47 ms).[28]

Absolute overall quantum yields (ϕ_{ov}) have been determined with an integrating sphere by exciting the samples into the ligand levels (λ_{ex} = 365 nm in solid state and 315 nm in DMF). They are related to the intrinsic quantum yields (i.e., determined upon excitation into the f-levels, ϕ_{Ln}) and the efficiency of the ligand-to-metal energy transfer (ϕ_{sen}):

$$\phi_{ov} = \phi_{sen} \times \phi_{Ln} \tag{3}$$

The experimental determination of ϕ_{Ln} is not easy, in view of the faint f−f oscillator strengths and overlap with the ligand absorption bands. However, ϕ_{Ln} can be evaluated from the observed and radiative lifetimes of $Eu(^5D_0)$. The latter can be computed in two ways. The first one involves using eq 4, by taking the magnetic dipole $^5D_0 \rightarrow {}^7F_1$ transition as reference with a spontaneous emission rate, A_{01}, equal to 14.65 × n^3 s^{-1}, where n is the refractive index of the emitting medium.[33] The rate of the spontaneous emission, A_{rad}, can be determined by summing up all A_{0J}:[34]

$$A_{rad} = \sum_J A_{0J} = A_{01} \sum_J \frac{\tilde{\nu}_{01}}{\tilde{\nu}_{0J}} \times \frac{S_{0J}}{S_{01}} \tag{4}$$

where S_{01} and S_{0J} are the corrected integrated intensities of the $^5D_0 \rightarrow {}^7F_1$ and $^5D_0 \rightarrow {}^7F_J$ (J = 2, 4) transitions, and $\tilde{\nu}_{01}$, $\tilde{\nu}_{0J}$ are their barycenter energies, respectively. Thus, by knowing the value of $A_{rad} = 1/\tau_{rad}$, one can calculate ϕ_{Ln}:

$$\phi_{Ln} = \left(\frac{A_{rad}}{A_{rad} + A_{nr}}\right) = \frac{\tau_{obs}}{\tau_{rad}} \tag{5}$$

Table 5. Intensity Parameters $\Omega_{2,4}$, Radiative (A_{rad}), Nonradiative (A_{nr}) Decay Rates, Intrinsic Quantum Yield (ϕ_{Ln}), Sensitization Efficiency (ϕ_{sen}), and Overall Quantum Yield (ϕ_{ov}) Values of the Eu^{III} Complexes at 298 K[a]

	$NBu_4[Eu(BTFA)_4]$			$(NBu_4[EuL])_2$		
		DMF (2×10^{-6} M)			DMF (1×10^{-6} M)	
parameter	solid[b]	eq 4[b]	eq 6[c]	solid[b]	eq 4[b]	eq 6[c]
Ω_2 (10^{-20} cm^{-2})	27.1	30.3		21.9	24.1	
Ω_4 (10^{-20} cm^{-2})	7.41	8.46		8.38	7.46	
τ_{obs} (μs)	730 ± 5	636 ± 1		710 ± 2	717 ± 1	
τ_{rad} (μs)	1030	924	870	1208	1135	1070
A_{rad} (s^{-1})	971	1083	1155	828	881	934
A_{nr} (s^{-1})	399	490	417	581	513	461
ϕ_{Ln} (%)	71	69	73	59	63	67
ϕ_{ov} (%)	60 ± 9	30 ± 5		51 ± 8	31 ± 5	
ϕ_{sen} (%)	85	44	41	87	49	46

[a]Estimated uncertainties: ±5% (Ω_J), ±12% (τ_{rad}, ϕ_{Ln}), and ±16% (ϕ_{sen}). [b]Relevant data calculated using eq 4. [c]Relevant data calculated using eq 6.

dx.doi.org/10.1021/ic500966z | Inorg. Chem. 2014, 53, 8407−8417

The second procedure is easier, in that it relies on the following simplified formula:[35]

$$A_{rad} = A_{01} \times n^3 \times \frac{S_{tot}}{S_{01}} \quad (6)$$

where S_{tot} is the total integrated and corrected emission intensity from the $^5D_0$ level. Data reported in Table 5 and determined according to these two procedures for the two DMF solutions (n = 1.430) agree to within ±6% (except A_{nr}, which is calculated as a difference), which constitutes a good test for eq 6. Solid-state data could not be calculated with eq 6, because the exact refractive index is not known. It is clear from Table 5 that both Eu^{III} complexes have higher ϕ_{ov} values in solid state than in DMF solution, and since the observed lifetimes do not differ substantially, this is almost entirely due to much smaller sensitization efficiencies in solution, possibly arising from collisional ligand deactivation before energy transfer. As expected, the ϕ_{ov} and τ_{obs} values for $NBu_4[Eu(BTFA)_4]$ in solid state are larger than those for $[Eu(BTFA)_3(H_2O)_2]$ (ϕ_{ov} = 30%, τ_{obs} = 380 μs).[32] Furthermore, the corresponding values for $(NBu_4[EuL])_2$ are among the largest reported for anhydrous dinuclear bis(β-diketonates)[12−14] (see Table S4 in the Supporting Information).

We have also tested the sensitization efficiency of the ligand H_4L for Tb^{III} ions. Photoluminescence studies were conducted in solid state and in DMF solution. When excited at 365 nm (solid state) or 315 nm (DMF), $(NBu_4[TbL])_2$ displays characteristic emission due to the transitions $^5D_4 \rightarrow {}^7F_6$ (488 nm), $^5D_4 \rightarrow {}^7F_5$ (545 nm), $^5D_4 \rightarrow {}^7F_4$ (585 nm), $^5D_4 \rightarrow {}^7F_3$ (616 nm), and $^5D_4 \rightarrow {}^7F_{2-0}$ (644 nm). Some residual emission

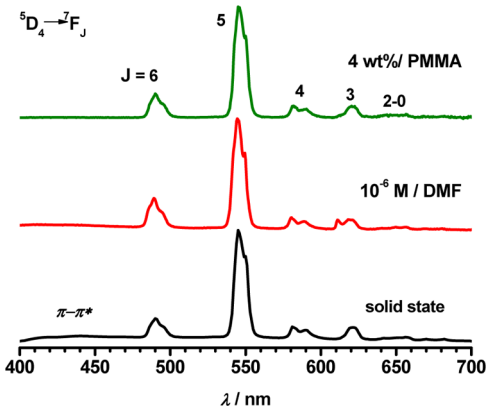

Figure 7. Corrected emission spectra of $(NBu_4[TbL])_2$ at 298 K, in solid state (λ_{ex} = 365 nm), 10^{-6} M in DMF (λ_{ex} = 315 nm), and 4 wt % doped in PMMA (λ_{ex} = 315 nm); vertical scales are arbitrary units.

from the ligand can also be seen at ∼450 nm (Figure 7). The $^5D_4$ lifetime is found to be very short (<50 μs, below the detection limit of our instrument) and no quantum yield value could be measured due to insufficient emission intensity. Such a situation can be explained in terms of the small energy difference between the triplet state of L^{4-} (21 320 cm^{-1}) and the $Tb(^5D_4)$ state (∼20 400 cm^{-1}), which facilitates efficient back energy transfer.

Modeling of the Photophysical Parameters and Energy Transfer Processes. The experimental photophysical parameters of the Eu^{III} complexes can now be compared with those obtained from theoretical calculations based on the Sparkle/AM1 model, which are given in Table 6 for both the dimeric and polymeric structures of the new chelate. Calculated

Table 6. Theoretical Judd−Ofelt Parameters and Luminescence Parameter Values Derived from the Optimized Sparkle/AM1 Model for the Dimeric and Polymeric Structures of the Eu^{III} Podate[a]

parameter	$(NBu_4[EuL])_2$	$(NBu_4[EuL])_n$
Ω_2 (10^{-20} cm^{-2})	21.1	15.1
Ω_4 (10^{-20} cm^{-2})	5.56	5.33
Ω_6 (10^{-20} cm^{-2})	0.30	0.37
A_{rad} (s^{-1})	772	586
τ_{rad} (μs)	1295	1706
A_{nr} (s^{-1})	636.4	1050.3
ϕ_{Ln} (%)	55	36
ϕ_{sen} (%)	99	99
ϕ_{ov} (%)	54	35

[a]Estimated uncertainties: ±5%.

parameters Ω_2, A_{rad}, A_{nr}, ϕ_{Ln}, and ϕ_{ov} for the dimeric species are in very good (±4%−9%) agreement with the experimental values obtained for the solid-state sample of $(NBu_4[EuL])_2$. On the other hand, theoretical values of the same parameters for the polymeric structure are off by ±30%−70%, which constitutes a strong argument in favor of the dimeric structure in the solid state. The discrepancies for the polymeric structure essentially arise from a much smaller Ω_2 parameter (15×10^{-20} cm^2 versus 21×10^{-20} cm^2; experimental value: 22×10^{-20} cm^2).

Modeling of the sensitization process in the investigated Eu^{III} complexes was made according to Figure 8 for $(NBu_4[EuL])_2$

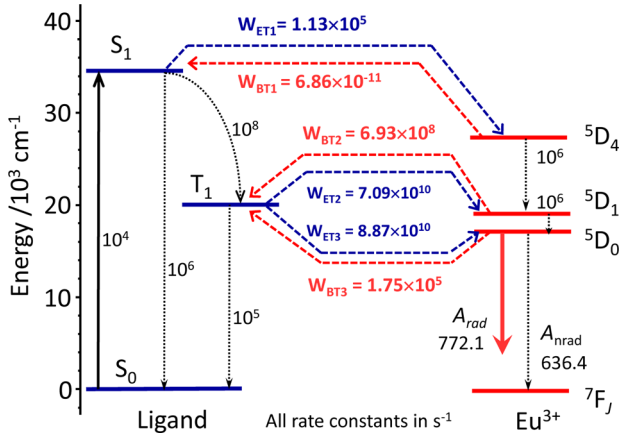

Figure 8. Schematic energy level diagram, energy transfer processes, and transfer rates for $(NBu_4[EuL])_2$.

and Figure S4 in the Supporting Information for the polymeric structure. Direct transfers from both the ligand singlet state (S_1, calculated energy = 34 890 cm^{-1}) and triplet state (T_1, 20 030 cm^{-1}) have been taken into consideration. The potential receiving levels of Eu^{III}, taking into account the selection rules and the $^7F_{0,1}$ population at room temperature, are $^5D_4$ (∼27 500 cm^{-1}), $^5D_1$ (∼19 000 cm^{-1}), and $^5D_0$ (∼17 250 cm^{-1}). Intramolecular energy transfer, back-transfer rates, and the percentage contribution of each process to the overall energy transfer are presented in Table 7 for the dimer and Table S5 in the Supporting Information for the polymer. The simulation points to a rather slow transfer from the singlet state onto

dx.doi.org/10.1021/ic500966z | Inorg. Chem. 2014, 53, 8407−8417

Table 7. Calculated Values of Intramolecular Energy Transfer, Back-Transfer Rates, and % Contribution of Each Process to the Overall Energy Transfer for $(NBu_4[EuL])_2$[a]

ligand state → 4f state (cm^{-1})	R_L (Å)	transfer rate (s^{-1})	back-transfer rate (s^{-1})	contribution (%)
S_1(34889) → $^5D_4$(27586)	3.5453	1.13×10^5	6.86×10^{-11}	7.1×10^{-5}
T_1(20033) → $^5D_1$(19027)	3.3948	7.09×10^{10}	6.93×10^8	44.2
T_1(20033) → $^5D_0$(17293)	3.3948	8.87×10^{10}	1.75×10^5	55.8

[a]The R_L value is the distance from the donor state located on the organic ligands and the Eu^{III} ion nucleus.

$Eu(^5D_4)$, $>10^5$ slower than the transfer from the triplet state to either $^5D_1$ or $^5D_0$. However, regarding the latter, back transfer processes are much faster than for $^5D_4$; nevertheless, the S_1-to-$^5D_4$ pathway plays a negligible role. The transfer to $^5D_0$ is 25% faster, compared to $^5D_1$; in addition, back transfer from $^5D_1$ is much faster than from $^5D_0$, so that the T_1-to-$^5D_0$ process accounts for slightly more than half (55.8%) of the total energy transfer.

Luminescence Properties of Hybrid Materials. The attractive photophysical properties of the new dimeric podate $(NBu_4[EuL])_2$ prompted us to produce luminescent thin films for photonic applications by doping it into an optically transparent polymeric matrix, PMMA. First, we have tested the influence of the doping concentration on the photophysical parameters. Spectra are shown in Figure 9 and corresponding

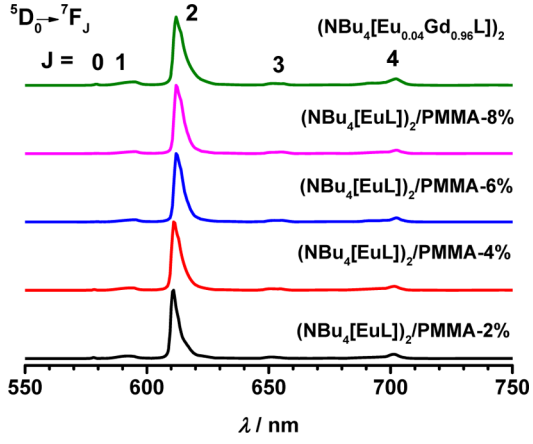

Figure 9. Corrected emission spectra of $(NBu_4[EuL])_2$-doped PMMA films (2–8 wt %) and of $(NBu_4[Gd_{0.96}Eu_{0.04}L])_2$ at 298 K, excitation wavelength = 365 nm, vertical scales given in arbitrary units.

quantitative data are listed in Table 8. All emission spectra are the same and similar to the one of the parent podate; this situation also prevails for excitation spectra (Figure S5 in the Supporting Information). The lifetime τ_{obs} of the 2 wt % hybrid material is equal to the one of the pure podate, within experimental errors, but it decreases to 610 μs with increasing concentration, a possible effect of concentration quenching. On the other hand, the quantum yields display a complex behavior, increasing from the $(NBu_4[EuL])_2$ value for the 2 wt % sample to 69% for the 4 wt % sample and then slightly decreasing to reach 61% for the 8 wt % sample. However, one must note that these values are almost within experimental errors, except for the 4 wt % sample. The major contribution to the emission spectra comes from the hypersensitive transition $^5D_0 \rightarrow ^7F_2$, which represents 82%–86% of the entire emission intensity, leading to good chromaticity of the materials. The intensity ratio R is in the range of 22.2–24.8 (see Table S6 in the Supporting Information) for PMMA samples, that is ~35%–50% larger than for solid state $(NBu_4[EuL])_2$ (16.5). This observation can be rationalized in terms of some interaction associated with the complex upon incorporation into the microcavities of the PMMA matrix, which probably results in the polarization of the complex and increases the probability for the electric dipole allowed transition.[36] This effect is also reflected by the larger values of Ω_2 ($(24.00–36.30) \times 10^{-20}$ cm^2) in PMMA, compared to $(NBu_4[EuL])_2$ in solid state (21.90×10^{-20} cm^2). Another consequence stems from the incorporation of the luminescent centers into PMMA. When examining the parameters listed in Tables 5 and 8, one realizes that the ~30% increase in ϕ_{ov} observed in going from the bulk podate to the 4 wt % PMMA sample is almost entirely due to an increase in ϕ_{Ln} (+25%), whereas the sensitization efficiency only increases marginally (+5%) and this increase is within experimental errors. This means that the effect of the matrix is mostly "mechanical" in that immobilization of the sample in the pores results in less fluxionality for the complex and is probably responsible for the decrease in nonradiative deactivation processes. It is noteworthy that a PMMA film doped with 4 wt % of the Tb^{III} dimeric podate is also more luminescent than the parent compound and that its quantum yield, although modest, could be measured, ϕ_{ov} = 1.5% ± 0.5%.

In order to try to further unravel the influence of the PMMA matrix on the photophysical parameters, we have synthesized the heterobimetallic complex $(NBu_4[Eu_{0.04}Gd_{0.96}L])_2$ as a reference. EDS analysis ascertains its stoichiometry (see Figure S6 and Table S7 in the Supporting Information) and both its excitation (Figure S5 in the Supporting Information) and emission spectra (Figure 9) are fairly similar to those of the pure Eu^{III} chelate or of the PMMA-doped samples. On the other hand, the Gd^{III} complexes surrounding the emitting Eu^{III} centers in $(NBu_4[Eu_{0.04}Gd_{0.96}L])_2$ have mixed effect on ϕ_{ov} and τ_{obs} values. Compared to $(NBu_4[EuL])_2$, the bimetallic complex contains only 4% of emitting species for the same number of ligands, hence one would expect a ϕ_{ov} value of ~2%, (4% of 51%), but it is 4.5 times larger. Furthermore, because of the dilution of emitting Eu^{III} centers by the nonemitting Gd^{III}, which increases the Eu^{III}–Eu^{III} intermolecular distances and reduces nonradiative energy transfer between the Eu^{III} ions, a longer $^5D_0$ lifetime than in $(NBu_4[EuL])_2$ is expected. However, an opposite effect is observed, with τ_{obs} decreasing by ~10%. These facts can be explained in terms of intermolecular energy transfer from the ligand-excited Gd^{III} podate to the nearby Eu^{III} ions, possibly through space (columinescence), hence increasing the overall quantum yield. At the same time, the probability of back-transfer from the $^5D_0$ state of Eu^{III} to the low-lying triplet states of the L^{4-} moieties could be enhanced in view of their larger number, thereby reducing the lifetime.

Luminescent functional nanofibers have drawn significant attention recently in areas such as light-emitting diodes, full color displays, lasers, and data storage. Luminescence in polymeric nanofibers can be induced by doping them with quantum dots (QDs) or luminescent transition-metal ions or complexes. In particular, a sizable amount of work has been done on Eu^{III} and Er^{III} composites,[37] mostly because photostability of the composite fibers is usually improved, compared

dx.doi.org/10.1021/ic500966z | Inorg. Chem. 2014, 53, 8407–8417

Table 8. Experimental Intensity Parameters $\Omega_{2,4}$ and Luminescence Parameters for PMMA Films (Thickness ≈ 0.6−0.9 mm) and Nanowires (o.d. ≈ 200−300 nm) Doped with Various Amounts of the Eu^{III} Podate, at 298 K[a]

		$(NBu_4[EuL])_2$/PMMA				
parameter	$(NBu_4[Eu_{0.04}Gd_{0.96}L])_2$	(2%)	(4%)	(4%)[b]	(6%)	(8%)
Ω_2 (10^{-20} cm^{-2})	22.1	24.0	29.9	29.9	33.0	36.3
Ω_4 (10^{-20} cm^{-2})	8.55	6.64	7.38	7.38	7.77	7.88
τ_{obs} (μs)	632 ± 4	712 ± 4	701 ± 4	697 ± 3	660 ± 4	615 ± 4
τ_{rad} (μs)	1582	1236	949	949	868	798
A_{rad} (s^{-1})	838	811	1053	1053	1153	1253
A_{nr} (s^{-1})	744	594	373	373	363	373
ϕ_{Ln} (%)	40	58	74	73	76	77
ϕ_{sen} (%)	22.5	88	91	94	83	79
ϕ_{ov} (%)	9 ± 1	51 ± 9	67 ± 10	69 ± 10	63 ± 9	61 ± 9

[a]Estimated uncertainties: ±5% (Ω_J), ±12% (τ_{rad}, ϕ_{Ln}), and ±16% (ϕ_{sen}). [b]PMMA wires.

to that of bulk material.[38] We have consequently produced one-dimensional nanostructures by electrospinning a 4-wt %-doped PMMA film. The resulting nanowires have diameters in the range of 200−300 nm and are shown in Figure 10. The spinning process has no detrimental effect on photoluminescent properties as shown in Table 8. In particular, the overall quantum yield is the same as that of the parent film, within experimental errors.

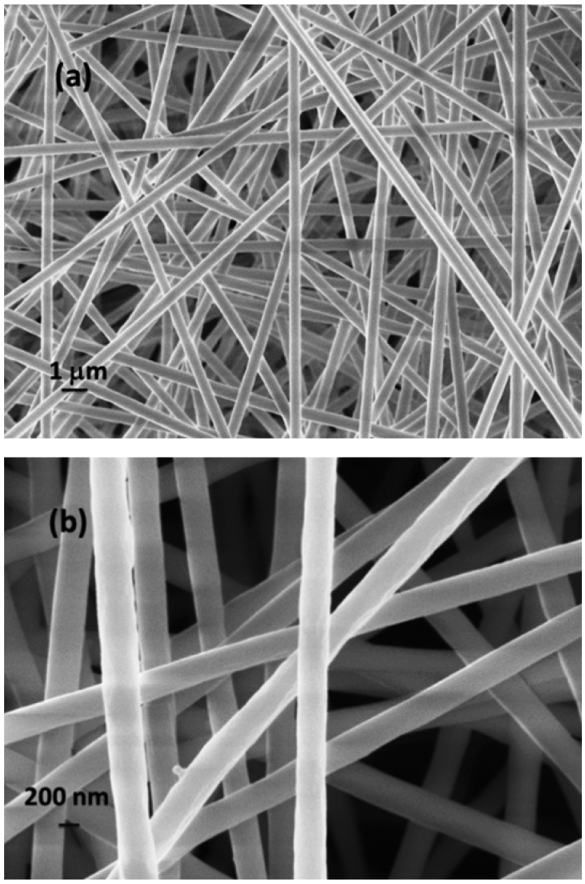

Figure 10. SEM images of nanowires of $(NBu_4[EuL])_2$-doped PMMA resin (4 wt %): (a) low magnification, scale bar = 1 μm; (b) high magnification, scale bar = 200 nm.

CONCLUSION

A new highly luminescent Eu^{III} podate based on a tetrakis(β-diketonate) ligand containing four BTFA units has been synthesized and characterized. A dimeric structure is predicted for this chelate by Sparkle/AM1 calculations and is backed by mass-spectral data and by comparison between experimental and calculated photoluminescence data. The $^5D_0$ lifetime and overall quantum yield (in solid state) obtained for the Eu^{III} podate were found to be the highest values reported so far in the literature, among dinuclear Eu^{III} bis(β-diketonates). Most importantly, the Eu^{III} podate can be easily doped into a PMMA matrix, resulting in highly luminescent films and, after electrospinning, in one-dimensional nanowires, the overall quantum yields of which reach 67%−69% for a doping concentration of 4 wt %. Doped thin films with thicknesses of ∼0.8 mm absorb more than 95% of the incident radiation and emit a highly monochromatic red light that can be easily seen by the naked eye even under natural day light (Figure 11). Thus, these films act as wavelength-converting materials, which could be provided in several practical applications such as luminescent solar concentrators for photovoltaic cells, UV sensors for sunlight, or various analytical sensors and

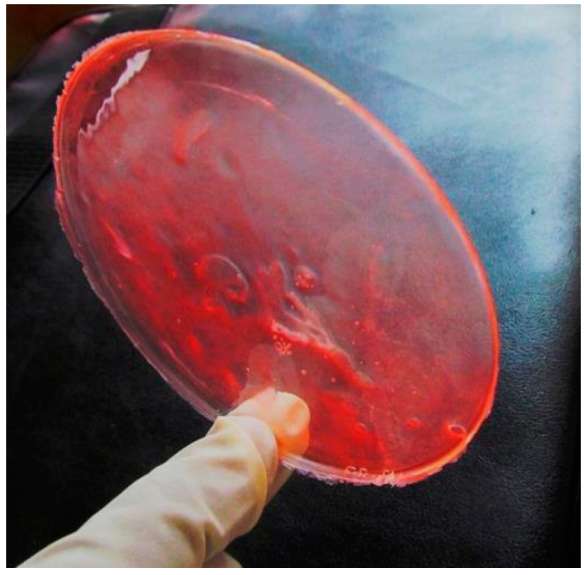

Figure 11. Photograph of a PMMA film doped with 4 wt % of $(NBu_4[EuL])_2$ under natural daylight.

dx.doi.org/10.1021/ic500966z | Inorg. Chem. 2014, 53, 8407−8417

biosensors. Further work along these lines is progressing in our laboratories.

■ ASSOCIATED CONTENT

Supporting Information

Detailed experimental procedure adopted for theoretical calculations, TGA for complexes, PL data, EDS analysis results, crystal data, collection, and structure refinement parameters in PDF format, crystal structure data in CIF format. This material is available free of charge via the Internet at http://pubs.acs.org.

■ AUTHOR INFORMATION

Corresponding Authors

*E-mail: drbijusilvanose@gmail.com (S. Biju).
*E-mail: jean-claude.bunzli@epfl.ch (J.-C. G. Bünzli).
*E-mail: hkk777@korea.ac.kr (H. K. Kim).

Notes

The authors declare no competing financial interest.

■ ACKNOWLEDGMENTS

This research was supported by the World Class University Program funded by the Ministry of Education, Science, and Technology through the National Research Foundation of Korea (Grant No. R31-2012-000-10035-0), and by a grant from Korea University (2010). One of the authors (S.B.) thanks the Collegiate Education Department and the Department of Higher Education, Government of Kerala, India, for granting leave without allowance for doing postdoctoral research. The Brazilian author (R.O.F.) appreciates the financial support from the Brazilian agencies, institutes and networks (CNPq, CAPES, FAPITEC-SE, and INCT/INAMI).

■ REFERENCES

(1) Binnemans, K. *Handbook on the Physics and Chemistry of Rare Earths*; Gschneidner, K. A., Jr., Bünzli, J.-C. G., Pecharsky, V. K., Eds.; North Holland: Amsterdam, 2005; Vol. 35, Chapter 225, pp 107−272.
(2) Ma, Y.; Wang, Y. *Coord. Chem. Rev.* **2010**, *254*, 972−990.
(3) Tanner, P. A. *Chem. Soc. Rev.* **2013**, *42*, 5090−5101.
(4) (a) Kido, J.; Okamoto, Y. *Chem. Rev.* **2002**, *102*, 2357−2368. (b) Binnemans, K. *Chem. Rev.* **2009**, *109*, 4283−4374. (c) de Bettencourt-Dias, A. *Dalton Trans.* **2007**, 2229−2241.
(5) Charles, R. G.; Riedel, E. P. *J. Inorg. Nucl. Chem.* **1966**, *28*, 3005−3018.
(6) Bünzli, J.-C. G.; Chauvin, A.-S. *Handbook on the Physics and Chemistry of Rare Earths*; Bünzli. J.-C. G., Pecharski, V. K., Eds.; Elsevier Science Publishers: Amsterdam, 2014; Vol. 44, Chapter 261, pp 169−281.
(7) (a) Wang, X.; Wang, T.; Tian, X.; Wang, L.; Wu, W.; Luo, Y.; Zhang, Q. *Sol. Energy* **2011**, *85*, 2179−2184. (b) Wang, T.; Zhang, J.; Ma, W.; Luo, Y.; Wang, L.; Hu, Z.; Wu, W.; Wang, X.; Zou, G.; Zhang, Q. *Sol. Energy* **2011**, *85*, 2571−2579. (c) de Sá, G. F.; Alves, S., Jr; da Silva, B. J. P.; da Silva, E. F., Jr. *Opt. Mater.* **1998**, *11*, 23−28.
(8) Reddy, M. L. P.; Divya, V.; Pavithran, R. *Dalton Trans.* **2013**, *42*, 15249−15262.
(9) (a) Bruno, S. M.; Ferreira, R. A. S.; Almeida Paz, F. A.; Carlos, L. D.; Pillinger, M.; Ribeiro-Claro, P.; Gonçalves, I. S. *Inorg. Chem.* **2009**, *48*, 4882−4895. (b) Lima, N. B. D.; Goncalves, S. M. C.; Junior, S. A.; Simas, A. M. *Sci. Rep.* **2013**, *3*, 2395−2398.
(10) (a) Yuan, J.; Wang, G.; Kimura, H.; Matsumoto, K. *Anal. Biochem.* **1997**, *254*, 283−287. (b) Matsumoto, K.; Kimura, H.; Kon, N.; Yoshida, K.-i.; Abo, M.; Yoshimura, E. *Anal. Sci.* **2013**, *29*, 971−977.
(11) Liu, S.; He, P.; Wang, H.; Shi, J.; Gong, M. *Mater. Chem. Phys.* **2009**, *116*, 654−657.
(12) (a) Liu, S.; He, P.; Wang, H.; Shi, J.; Gong, M. *Inorg. Chem. Commun.* **2009**, *12*, 506−508. (b) Shi, J.; Hou, Y.; Chu, W.; Shi, X.; Gu, H.; Wang, B.; Sun, Z. *Inorg. Chem.* **2013**, *52*, 5013−5022.
(13) (a) Li, H.-F.; Yan, P.-F.; Chen, P.; Wang, Y.; Xu, H.; Li, G.-M. *Dalton Trans.* **2012**, *41*, 900−907. (b) Albrecht, M.; Schmid, S.; Dehn, S.; Wickleder, C.; Zhang, S.; Bassett, A. P.; Pikramenou, Z.; Frohlich, R. *New J. Chem.* **2007**, *31*, 1755−1762.
(14) He, P.; Wang, H. H.; Liu, S. G.; Shi, J. X.; Wang, G.; Gong, M. L. *Inorg. Chem.* **2009**, *48*, 11382−11387.
(15) Biju, S.; Eom, Y. K.; Bünzli, J.-C. G.; Kim, H. K. *J. Mater. Chem. C* **2013**, *1*, 6935−6944.
(16) (a) Eliseeva, S. V.; Bünzli, J.-C. G. *Chem. Soc. Rev.* **2010**, *39*, 189−227. (b) Feng, J.; Zhang, H. *Chem. Soc. Rev.* **2013**, *42*, 387−410.
(17) Carlos, L. D.; Ferreira, R. A. S.; de Zea Bermudez, V.; Julian-Lopez, B.; Escribano, P. *Chem. Soc. Rev.* **2011**, *40*, 536−549.
(18) (a) Lunstroot, K.; Driesen, K.; Nockemann, P.; Viau, L.; Mutin, P. H.; Vioux, A.; Binnemans, K. *Phys. Chem. Chem. Phys.* **2010**, *12*, 1879−1885. (b) Hasegawa, Y.; Yamamuro, M.; Wada, Y.; Kanehisa, N.; Kai, Y.; Yanagida, S. *J. Phys. Chem. A* **2003**, *107*, 1697−1702.
(19) McCoy, C. P.; Stomeo, F.; Plush, S. E.; Gunnlaugsson, T. *Chem. Mater.* **2006**, *18*, 4336−4343.
(20) Xia, Y.; Yang, P.; Sun, Y.; Wu, Y.; Mayers, B.; Gates, B.; Yin, Y.; Kim, F.; Yan, H. *Adv. Mater.* **2003**, *15*, 353−389.
(21) (a) Li, D.; Xia, Y. *Adv. Mater.* **2004**, *16*, 1151−1170. (b) Darrell, H. R.; Iksoo, C. *Nanotechnology* **1996**, *7*, 216.
(22) (a) *Crysalis PRO, Agilent Technologies, release 1.171.36.24*, 2012. (b) Sheldrick, G. M. *Acta Crystallogr., Sect. A* **2008**, *64*, 112−122.
(23) Aebischer, A.; Gumy, F.; Bünzli, J.-C. G. *Phys. Chem. Chem. Phys.* **2009**, *11*, 1346−1353.
(24) Guan, J.; Chen, B.; Sun, Y.; Liang, H.; Zhang, Q. *J. Non-Cryst. Solids* **2005**, *351*, 849−855.
(25) (a) Xu, J.; Radkov, E.; Ziegler, M.; Raymond, K. N. *Inorg. Chem.* **2000**, *39*, 4156−4164. (b) Biju, S.; Gopakumar, N.; Bünzli, J. C. G.; Scopelliti, R.; Kim, H. K.; Reddy, M. L. P. *Inorg. Chem.* **2013**, *52*, 8750−8758.
(26) (a) Binnemans, K.; Van Deun, R.; Gorller-Walrand, C.; Collinson, S. R.; Martin, F.; Bruce, D. W.; Wickleder, C. *Phys. Chem. Chem. Phys.* **2000**, *2*, 3753−3757. (b) Biju, S.; Raj, D. B. A.; Reddy, M. L. P.; Kariuki, B. M. *Inorg. Chem.* **2006**, *45*, 10651−10660. (c) Raj, D. B. A.; Biju, S.; Reddy, M. L. P. *Inorg. Chem.* **2008**, *47*, 8091−8100.
(27) Blasse, G. *Inorg. Chim. Acta* **1988**, *142*, 153−154.
(28) Bünzli, J.-C. G.; Yersin, J.-R. *Helv. Chim. Acta* **1982**, *65*, 2498−2506.
(29) Eliseeva, S. V.; Kotova, O. V.; Gumy, F.; Semenov, S. N.; Kessler, V. G.; Lepnev, L. S.; Bünzli, J.-C. G.; Kuzmina, N. P. *J. Phys. Chem. A* **2008**, *112*, 3614−3626.
(30) (a) Judd, B. R. *Phys. Rev.* **1962**, *127*, 750−761. (b) Ofelt, G. S. *J. Chem. Phys.* **1962**, *37*, 511−520.
(31) Divya, V.; Freire, R. O.; Reddy, M. L. P. *Dalton Trans.* **2011**, *40*, 3257−3268.
(32) de Mello Donegá, C.; Junior, S. A.; de Sá, G. F. *J. Alloys Compd.* **1997**, *250*, 422−426.
(33) Görller-Walrand, C.; Fluyt, L.; Ceulemans, A.; Carnall, W. T. *J. Chem. Phys.* **1991**, *95*, 3099−3106.
(34) Araújo, A. A. S.; Brito, H. F.; Malta, O. L.; Matos, J. R.; Teotonio, E. E. S.; Storpirtis, S. l.; Izumi, C. M. S. *J. Inorg. Biochem.* **2002**, *88*, 87−93.
(35) (a) Werts, M. H. V.; Jukes, R. T. F.; Verhoeven, J. W. *Phys. Chem. Chem. Phys.* **2002**, *4*, 1542−1548. (b) Chauvin, A. S.; Gumy, F.; Imbert, D.; Bünzli, J.-C. G. *Spectrosc. Lett.* **2004**, *37*, 517−532; (c) Chauvin, A. S.; Gumy, F.; Imbert, D.; Bünzli, J.-C. G. *Spectrosc. Lett.* **2007**, *40*, 193 (Erratum). (d) Biju, S.; Reddy, M. L. P.; Cowley, A. H.; Vasudevan, K. V. *J. Mater. Chem.* **2009**, *19*, 5179−5187.
(36) Li, Q.; Li, T.; Wu, J. *J. Phys. Chem. B* **2001**, *105*, 12293−12296.
(37) Agarwal, S.; Greiner, A.; Wendorff, J. H. *Prog. Polym. Sci.* **2013**, *38*, 963−991.
(38) Yu, H.; Li, T.; Chen, B.; Wu, Y.; Li, Y. *J. Colloid Interface Sci.* **2013**, *400*, 175−180.